Chapter 4

GRB 030329 : Detailed Investigations of a Fireball Deep in the Non-Relativistic Phase of Evolution

Abstract

GRB 030329 displayed one of the brightest optical afterglows ever. The radio afterglow of the GRB still shines at low frequencies. In this Chapter, we present the low frequency radio observations of GRB 030329 afterglow for 1400 days after the burst. The afterglow was observed using Giant Metrewave Radio Telescope (India) at center frequencies of 1280 MHz, 610 MHz and 325 MHz.

We have studied the non-relativistic phase of the afterglow evolution and estimated the energy content and other physical parameters of the fireball. We have also attempted to look for the signature of counter jet in the afterglow light curves but we have not found any conclusive evidence for it. The fireball blast-wave is commonly assumed to be spherical during the non-relativistic phase which need not be true. A correct model for non-relativistic evolution of the fireball blast-wave should take into account Equal Time of Arrival surfaces. We have briefly discussed this issue also in this Chapter.

4.1 Introduction

GRB 030329 has been a very distinct event in many respects. Residing at a redshift of 0.1685 (Matheson et al., 2003) (distance of ~ 870 Mpc in the flat universe with $\Omega_m = 0.3, \Omega_\Lambda = 0.7$ and Hubble Constant = 65 km $s^{-1}Mpc^{-1}$) it is the second nearest GRB for which an afterglow has been observed (GRB 980425 at z = 0.0085 remains the nearest of the GRBs with measured redshifts since their discovery in 1960s). The afterglow GRB030329 is one with the longest followed up ever. The afterglow is seen at radio frequencies even after 1400 days since explosion. It was also the first GRB to have provided an unambiguous evidence of the long suspected association between GRBs and Supernovae e.g. (Galama et al., 1999).

GRB 030329 was detected and localized by the HETE-II satellite (Vanderspek et al., 2004) on 29th March 2003, at UT 11:37:14.7 and lasted more than 100s. The measured fluence, between 30-400 keV, for this burst was 1.1×10^{-4} erg cm^{-2} The (Soft X-ray Camera) SXC, an instrument on board HETE-II, localized the GRB at RA (J2000) = $10^h44^m49^s$ and Dec (J2000) = $+21°28'44''$ within an error circle of radius 2 arcmin. The burst light curve showed it to be double peaked. Fluence in the band 7-30 keV was 5.5×10^{-5} erg cm^{-2}. The burst was followed by an extremely bright X-ray afterglow, 1.4×10^{-10} erg cm^{-2} s^{-1} in 2-10 keV band, detected by RXTE ~ 5 h after the burst (Marshall and Swank 2003). Peterson and Price (2003) and Torii (2003) detected the bright optical afterglow in R band at ~ 13 mag, the brightest to date. A bright radio afterglow of 3.5 mJy at 8.46 GHz was detected by VLA Berger et al. (2003) on 2003 March 30.06 UT. Around 7 days after the burst the optical spectrum showed the signature of an underlying supernova emission, SN2003dh (Stanek et al., 2003; Hjorth et al., 2003; Matheson et al., 2003). The afterglow was subsequently followed in various optical, milli meter and radio wavelengths providing the richest temporal coverage of the transient in all the

wavebands (Lipkin et al., 2004; Tiengo et al., 2003; Sheth et al., 2003; Kuno et al., 2004; Berger et al., 2003; Resmi et al., 2005; Gorosabel et al., 2006)

Extended radio follow up of the afterglow have been earlier reported by Frail et al. (2005a); van der Horst et al. (2005) and by Resmi et al. (2005). These reports cover a period of up to 1 year post burst. We have further extended the temporal coverage of the afterglow using our low frequency radio follow up of GRB 030329 afterglow, up to $\sim$ 1400 days after the burst, using the Giant Metrewave Radio Telescope (GMRT) operated by the National Center for Radio Astrophysics (NCRA), Pune. These observations are reported in van der Horst et al. (2007). GRB 030329 is the first afterglow to be observed at a frequency as low as 610 MHz. We also attempted to observe the afterglow at 325 MHz, but were unable to detect it due to our sensitivity limit.

4.2 Radio observations using GMRT and analysis

The radio afterglow of GRB 030329 was first detected by GMRT at 1280 MHz on 31st March 2003, 2.3 days after the burst (Rao et al., 2003) with a flux of 0.33 mJy. The afterglow was followed up since then at 1280 MHz, 610 MHz and 325 MHz. The first year of observations of the radio afterglow have been reported by Resmi et al. (2005). In this Chapter we discuss in detail our subsequent observations, extending the coverage till 1400 days after the burst. We observed the afterglow at a total of 16 epochs (8 epochs at 1280 MHz, 6 epochs at 610 MHz and 2 epochs at 325 MHz) excluding the first year observations reported in Resmi et al. (2005) (9 epochs at 1280 MHz). We have used a bandwidth of 32 MHz for all these observations. One of the three possible flux calibrators, 3C48, 3C147 or 3C286, was observed at the beginning and end of each observing session for about 15 minutes, as a primary flux calibrator to which the flux scale was set. Radio sources 1125+261 and 1021+219

were used as phase calibrators at 1280 MHz and 610 MHz, respectively. The phase calibrator was observed for about 6 minutes before and after an observing scan of about 30 to 45 minutes on GRB 030329. The data thus recorded were then converted to FITS format and analyzed using Astronomical Image Processing System (AIPS). Fluxes of the individual sources were measured using a task 'jmfit' in AIPS.

We found some flux variation in sources in the field of GRB 030329, rms of which is maximum of 20 % and minimum of 10 %. At most 15 % of this variation appears to be correlated i.e. all the sources varying in same sense from one frame to another. This correlated variation can be attributed to calibration uncertainties. To correct for this correlated variation we followed following procedure.

For calibration of each frame observed at 1280 MHz we used a frame of the same field from the First Survey as a reference frame. For calibration of the field at 610 MHz we used one of our own observations, dated 2nd Sep. 2005, as a reference frame. We selected four sources in the field within $5'$ of the GRB 030329 position and measured their fluxes. Ratios of these measured fluxes to those sources in the reference frame were computed and averaged for each frame. The flux of the afterglow measured in each frame was then calibrated using this average of the flux ratios. The final fluxes are presented in Table 4.1.

4.3 Modeling the Multifrequency Radio Afterglow

According to the Fireball model the afterglow of a GRB is due to non-thermal synchrotron radiation emitted by shock accelerated electrons. The large amount of energy released during the burst, with a collimated outflow to start with, drives a powerful relativistic shock wave. As the shock wave propagates into the circum-burst medium it heats up the circum-burst medium to high temperatures. The electrons in the medium are accelerated to assume a power law energy distribution

Observing Dates	ΔT (days)	Frequency (MHz)	Flux (mJy)
2005 Jan 6.82	649.34	610	0.50 ± 0.11
2005 Feb 8.81	682.33	325	$< 1.5(3\sigma)$
2005 Feb 13.84	687.34	1280	0.85 ± 0.13
2005 Feb 21.71	695.23	610	0.47 ± 0.13
2005 Mar 10.77	712.29	1280	0.63 ± 0.06
2005 Mar 18.66	720.18	610	0.69 ± 0.13
2005 Jun 17.54	811.06	610	$< 1.1(3\sigma)$
2005 Jun 28.59	702.11	325	$< 1.8(3\sigma)$
2005 Jul 1.19	824.71	1280	0.46 ± 0.08
2005 Sep 2.99	888.51	610	0.68 ± 0.13
2005 Oct 8.20	923.72	1280	0.43 ± 0.08
2006 Jan 1.9	1009.42	1280	0.99 ± 0.08
2006 Jan 4.06	1011.58	610	1.04 ± 0.11
2006 Jul 27.44	1154.96	1280	0.31 ± 0.08
2007 Feb 13.77	1356.29	1280	0.39 ± 0.08
2007 Mar 28.73	1399.25	1280	0.64 ± 0.08

Table 4.1: Log of GMRT observations of GRB 030329. The measurement uncertainties are given at 1 σ level. The ΔT in column 2 corresponds to the time in days since the GRB.

($n_e(\gamma)\, d\gamma \propto \gamma^{-p}\, d\gamma$) with γ being Lorentz factor of the shocked electrons whose number density is n_e. These relativistic electrons gyrate in the post-shock magnetic field and emit synchrotron radiation which is seen as the afterglow of the GRB. The power law distribution of the electrons results in a power law spectrum of the afterglow. Meanwhile the shock wave decelerates as it propagates into the circum-burst medium. Assuming mass-energy conservation across the shock front, it has been shown that the Lorentz factor of the shock wave falls off as a power law with the radius of the Fireball. A detailed discussion of this can be found in Sari et al. (1998).

After a few weeks it is expected that the decelerating shock wave would become non-relativistic. Somewhat earlier, the sideways expansion of the initially tightly collimated outflow would become important and by the time of non-relativistic transition the shock wave becomes nearly spherical. In the non-relativistic phase the evolution of the shock wave can be described using the Sedov-von Neumann-Taylor (SNT) self similar solutions. A detailed description of this phase can be found in Frail, Waxman and Kulkarni (2000). Observations of the broadband afterglow during this phase can be used to estimate various physical parameters related to the explosion, such as the amount of energy released during the explosion, fractional amount of energy in the accelerated electrons and in the post-shock magnetic field and density of the circumburst medium. These parameters can also be estimated, independently, by modelling the evolution of the afterglow in the relativistic phase, but this suffers from uncertainties related to collimation geometry and relative orientation of the observer, problems that do not plague the non-relativistic phase.

Because most of the GRBs occur at cosmological distances they are not bright enough to be observed at late times and in fact most of them fade below the detection limits much before the start of the non-relativistic phase. GRB 030329 being one of the closest GRBs, provided us with an unique opportunity of late time observations deep into the non-relativistic phase.

The broadband afterglow of GRB 030329, from radio to X-ray frequencies, has been modeled with slight modifications of the standard relativistic blast wave model, assuming either a **double jet model** (Berger et al., 2003) or a **refreshed jet model** (Resmi et al., 2005). In both the models, the early-time optical and X-ray light curves are explained by a jet with a small opening angle of $\sim 5^{\circ}$. The double jet model assumes a co-aligned wider jet component ($\sim 20^{\circ}$) that carries the bulk

of the energy and produces the later-time light curves. In the refreshed jet model, the initial jet is re-energised by the central engine during its lateral expansion, to make it collimated to a wider opening angle. This refreshed jet then produces the late-time emission. Unfortunately, we can not distinguish between the two models with all the available data.

We have used $\sim$ 1400 days of broadband radio observations (610 MHz to 43.3 GHz) of the afterglow of GRB 030329, conducted by GMRT as well as those reported earlier by GMRT (Resmi et al., 2005), WSRT (van der Horst et al., 2005), and VLA and ATCA (Berger et al., 2003; Frail et al., 2005a), to model the dynamical evolution of the afterglow as well as to constrain explosion energy. The afterglow light curves show three distinct parts of evolution

Rise : The light curve is rising initially, with almost a similar rate of rise at all frequencies except at 610 MHz where we do not have observations during the rising phase of the afterglow. The afterglow takes longer to reach peak brightness at lower frequencies compared to that at higher frequencies.

Fall : After the peak, the light curve falls with almost a similar rates at all the frequencies.

Flattening : After about $\sim$ 80 days after the burst, the light curve at higher frequencies (22.5 GHz, 15 GHz, 8.4 GHz and 4.8 GHz), which had the peak brightness before $\sim$ 80 days, flattens out.

This behaviour of the light curves, can be explained as being due to the transition of the blast wave from relativistic into the non-relativistic phase of evolution at $\sim$ 60 days, the epoch of light curve flattening. (Frail et al., 2000; van der Horst et al., 2005; Resmi et al., 2005).

Along with our own GMRT observations at 325, 610 and 1280 MHz we have also used observations reported in literature (van der Horst et al., 2007) to model the broadband behaviour of the afterglow of GRB 030329. The data set forms a temporal baseline extending upto 1400 days since the burst and spectral range from 325 MHz to 43.3 GHz. We have used this data to model the dynamical evolution of the afterglow as well as to constrain the explosion energy. In Figure 4.1 we compare our model predictions with observations.

4.3.1 Physical Parameters

The fitted spectral parameters may now be used to derive the physical parameters of the explosion. The break frequencies and the peak flux, estimated deep in the non-relativistic phase, i.e. at a reference time $t_0 \gg t_{\rm NR}$, can be used to yield an estimate of the blast wave energy $E_{\rm ST}$ and the ambient baryon density n_i, using the Sedov-Taylor solution for the blast wave, in the manner adopted by Frail et al. (2000) (hereafter FWK00) for GRB970508. Two other physical parameters that determine the evolution of the radiation are the fraction of total energy in relativistic electrons ($\varepsilon_{\rm e}$) and in the post-shock magnetic field ($\varepsilon_{\rm B}$) respectively. In order to determine these four quantities, one requires the measurement of four spectral parameters, traditionally the three break frequencies and the flux normalisation. In the late phase, however, direct determination of the cooling frequency is difficult, since the afterglow is not detectable at frequencies above radio bands. We therefore express the physical parameters as a function of the ratio $\varepsilon_{\rm r} \equiv \varepsilon_{\rm e}/\varepsilon_{\rm B}$: $\varepsilon_{\rm r} = 1$ would signify an equipartition of energy between the magnetic field and the relativistic particles.

Following Eq. (5) of FWK00, we may then write the post-shock electron number density as

$$n = \varepsilon_{\rm r}\left(\frac{p-2}{p-1}\right)\frac{B_0^2}{8\pi\gamma_0 m_e c^2} \tag{4.1}$$

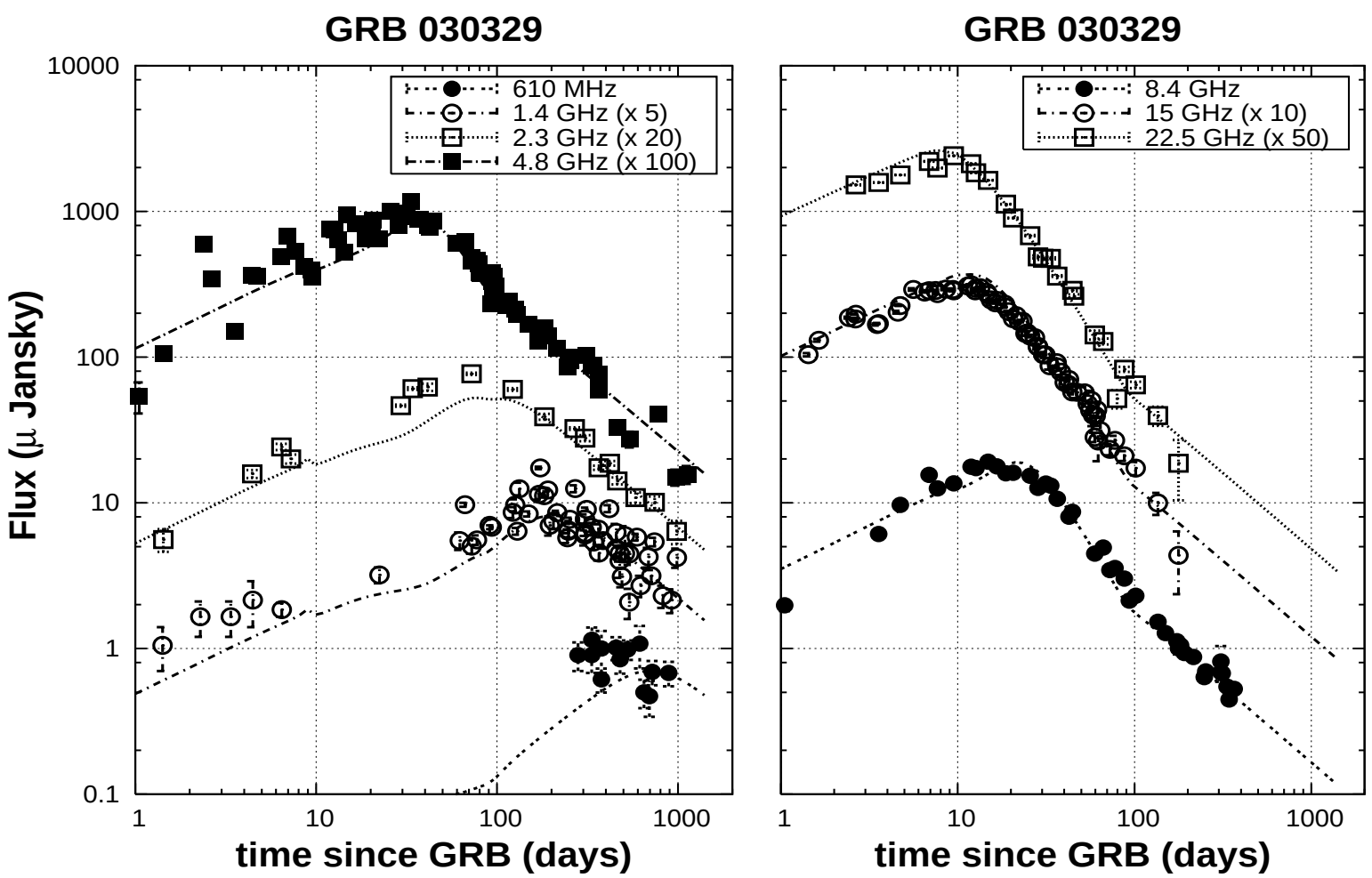

Figure 4.1: **Light curves of GRB 030329 afterglow :** GMRT observations of GRB 030329 radio afterglow compared with the predictions from Non-Relativistic evolution of the fireball. The observed data are denoted by points. The lines represent model predictions of the afterglow light curves. See the boxes at the top right in the both the panels to know corresponding frequencies.

We insert this in Eq. (A12) of FWK00, and invert their Eqs. (A10) to (A12) while making use of the relations (A6) to (A8). This yields the following set of expressions for the FWK00 model parameters:

$$\begin{aligned}\gamma_0 &= 88.3\, d_{28}^{2/17}\left(\frac{\varepsilon_r}{\eta_{10}}\right)^{2/17}\left(\frac{f_2^3}{f_3}\right)^{1/17} \\ &\quad\cdot\left[(p-2)^2(p+2)^3\right]^{1/17}\left(\frac{\nu_{m0,GHz}}{\nu_{a0,GHz}}\right)^{3(p+4)/34} F_{m0,mJy}^{1/17} \qquad (4.2)\\ r_0 &= 1.407\times10^{18}\ \mathrm{cm}\ \frac{d_{28}^{16/17}}{(1+z)}\left(\frac{\eta_{10}}{\varepsilon_r}\right)^{1/17}\left(\frac{f_2^7}{f_3^8}\right)^{1/17} \\ &\quad\cdot\left[\frac{(p+2)^7}{(p-2)}\right]^{1/17}\nu_{m0,GHz}^{(7p-6)/34}\nu_{a0,GHz}^{-7(p+4)/34}F_{m0,mJy}^{8/17} \qquad (4.3)\\ B_0 &= 4.58\times10^{-2}\ \mathrm{G}\ \frac{(1+z)}{d_{28}^{4/17}}\left(\frac{\eta_{10}}{\varepsilon_r}\right)^{4/17}\left(\frac{f_3}{f_2^3}\right)^{2/17} \\ &\quad\cdot\left[(p-2)^4(p+2)^6\right]^{-1/17}\nu_{m0,GHz}^{(5-3p)/17}\nu_{a0,GHz}^{3(p+4)/17}F_{m0,mJy}^{-2/17} \qquad (4.4)\\ n_i &= \frac{0.69\ \mathrm{cm}^{-3}}{1+X_H}\frac{(1+z)^2}{d_{28}^{10/17}}\left(\frac{\varepsilon_r}{\eta_{10}}\right)^{7/17}\left(\frac{f_3}{f_2^3}\right)^{5/17} \\ &\quad\cdot\frac{1}{(p-1)}\left[\frac{(p-2)^7}{(p+2)^{15}}\right]^{1/17}\nu_{m0,GHz}^{(8-15p)/34}\nu_{a0,GHz}^{15(p+4)/34}F_{m0,mJy}^{-5/17} \qquad (4.5)\end{aligned}$$

In the above, r_0 is the radius of the blast wave, B_0 is the post-shock magnetic field, and γ_0 is the lower cutoff of the power-law distribution of relativistic electron Lorentz factors, all at the reference time t_0. From these, the blast wave energy may be computed as:

$$\begin{aligned}E_{ST} &= n_i m_p\left(\frac{1+z}{t_0}\right)^2\left(\frac{r_0}{\xi}\right)^5 \qquad (4.6)\\ &= \frac{8.576\times10^{56}\ \mathrm{erg}}{(1+X_H)\xi^5 t_{0,d}^2}\frac{d_{28}^{70/17}}{(1+z)}\left(\frac{\varepsilon_r}{\eta_{10}}\right)^{2/17}\left(\frac{f_2^{20}}{f_3^{35}}\right)^{1/17}\frac{(p+2)}{(p-1)} \\ &\quad\cdot\left[(p-2)^2(p+2)^3\right]^{1/17}\nu_{m0,GHz}^{(10p-11)/17}\nu_{a0,GHz}^{-10(p+4)/17}F_{m0,mJy}^{35/17} \qquad (4.7)\end{aligned}$$

In Eq. (4.2) through (4.7), $\nu_{a0,GHz}$ and $\nu_{m0,GHz}$ are the two break frequencies, in GHz units, at the reference time $t_0 = t_{0,d}$ days. The expressions assume that $\nu_{a0,GHz} > \nu_{m0,GHz}$, which happens to be the case in GRB030329 at these late times. $F_{m0,mJy}$ is

the normalisation of the flux at an observing frequency $\nu \gg \nu_{\rm a}, \nu_{\rm m}$, expressed as

$$f_\nu(t = t_0)\ {\rm mJy}\ = F_{\rm m0,mJy} \left(\frac{\nu}{\nu_{\rm m0}}\right)^{-(p-1)/2} \tag{4.8}$$

z is the redshift of the burst and d_{28} the corresponding luminosity distance. The thickness of the post-shock emitting region at any time is assumed to be r/η, where r is the radius of the blast wave and $\eta = 10\eta_{10}$. f_2 and f_3 are integrals over the synchrotron function defined in FWK00; both are functions of p. The quantity ξ, close to unity, is an equation of state-dependent normalisation factor for the blast wave radius (FWK00). $X_{\rm H}$ represents the mass fraction of hydrogen in the circumburst medium, and we assume it to be of primordial value of ~ 0.75

Evaluating spectral parameters from the fitted model, one finds, at a reference time $t_0 = 500$ d, $\nu_{m0,\rm GHz} = 1.88 \times 10^{-3}$, $\nu_{a0,\rm GHz} = 0.775$ and $F_{m0,\rm mJy} = 37.9$. The fitted value of p is 2.1. Using $z = 0.1685$ and $d_{28} = 0.25$ for GRB030329 one then estimates

$$E_{\rm ST} = 0.82 \times 10^{51}\ {\rm erg} \left(\frac{\epsilon_r}{\eta_{10}}\right)^{0.12} \tag{4.9}$$

$$n_i = 1.3\ {\rm cm}^{-3} \left(\frac{\epsilon_r}{\eta_{10}}\right)^{0.41} \tag{4.10}$$

The blast wave radius at 500 d works out to be $r_0 = 0.3$ pc $(\epsilon_r/\eta_{10})^{-0.06}$. The corresponding postshock magnetic field is $B_0 = 0.057$ G $(\epsilon_r/\eta_{10})^{-0.24}$, and the lower cutoff of electron Lorentz factor distribution at that time is $\gamma_0 = 3.7(\epsilon_r/\eta_{10})^{0.12}$. These yield $\epsilon_e = \epsilon_r\epsilon_B = 0.15(\epsilon_r/\eta_{10})^{0.24}$.

4.4 Discussion

The observations of GRB 030329 afterglow give an unprecedented view on the non-relativistic evolution phase of a GRB blast wave, because of the wide range covered in both frequency and time. This gives us the opportunity to compare the physical

parameters that we have derived from the very late-time data with the physical parameters derived from the early-time data, when the blast wave was still extremely relativistic. From the emerging physical picture we put constraints on the emission from the counter jet, and we compare our findings with the results from VLBI measurements of the source size evolution.

4.4.1 Relativistic versus Non-Relativistic

We have fitted the available data of the radio afterglow of GRB 030329 separately, (1) only during the relativistic (< 40 days) phase, (2) only during the non-relativistic (> 100 days) phase, and (3) the entire data set with the earliest observation at 0.58 days (at 8.4 GHz) upto 1400 days after the burst.

In section 4.3.1 we calculated the total energy in the blast wave $E_{\rm ST}$ and the density of the circumburst medium n_i as functions of the ratio $\varepsilon_{\rm r} \equiv \varepsilon_{\rm e}/\varepsilon_{\rm B}$, assuming that the blast wave was in its non-relativistic phase.

Similarly, we have determined these parameters using only the relativistic evolution of the afterglow (< 40 days). Our best fit parameters indicate that the self-absorption frequency at 10.0 days after the burst was just below $\nu_m = 1.8 \times 10^{10}$ Hz, peak flux F_m at that epoch being $\sim$ 50.5 mJy and p = 2.1. The estimated physical parameters turn out to be : $E_K^{iso} = 5 \times 10^{50}\ \nu_{c_{13}}^{1/4}$ erg, $n = 0.6\ \nu_{c_{13}}^{3/4}$ cm^{-3}, $\epsilon_e = 0.2\ \nu_{c_{13}}^{1/4}$ and $\epsilon_B = 0.4\ \nu_{c_{13}}^{-5/4}$. Using the best fit jet break time $\sim$ 13 day the jet opening angle is estimated to be $\sim 21.5^\circ$ and hence $E_K^{corr} = 10^{50}\ \nu_{c_{13}}^{1/4}$.

The entire data set can be used to estimate the epoch of non-relativistic transition which turns out to be $\sim$ 60 days. The best fit spectral parameters turn out to be slightly different from the 'only relativistic' best fit parameters and hence the resultant physical parameters : $E_K^{iso} = 5 \times 10^{50}\ \nu_{c_{13}}^{1/4}$ erg, $n = 1.0\ \nu_{c_{13}}^{3/4}$ cm^{-3}, $\epsilon_e = 0.13\ \nu_{c_{13}}^{1/4}$ and $\epsilon_B = 0.6\ \nu_{c_{13}}^{-5/4}$. Using the best fit jet break time $\sim$ 13 day the jet

opening angle is estimated to be $\sim 23^{\circ}$ and hence $E_K^{corr} = 10^{50}\ \nu_{c_{13}}^{1/4}$.

Our estimates of beaming corrected energy using only the relativistic phase of afterglow turns out to be smaller by a factor of 8 compared to E_{ST} using non-relativistic phase while estimated ambient density in both the phases of evolution turns out be comparable.

Frail et al. (2005b) modeled the first year of observations with the VLA and ATCA, and found a total kinetic energy of 9.0×10^{50} ergs; using only the data before 64 days they derive an energy of 6.7×10^{50} ergs (see also Berger et al., 2003), a factor of ~ 7 larger than our E_K^{corr}; and using only the data after 50 days they find an energy of 7.8×10^{50} ergs, similar to our estimates of $E_{\rm ST}$. In these models the range for the circumburst density is $\sim 1 - 3\,{\rm cm}^{-3}$, a bit larger than our values. Granot et al. (2005) also determine the energy and density with their models, and find the collimation corrected energy which is larger by a factor of 4 compared to our estimates. Their value for the density is, however, an order of magnitude larger, but they note that this can be attributed to the fact that the density depends strongly on the precise value of $\nu_{\rm a}$ and $\nu_{\rm m}$.

Given the differences in the methods used by different authors and the uncertainties in the assumptions made to estimate these numbers, they can all be considered to be comparable. It is not possible to make any definite statements about significant differences in energies derived from the relativistic and non-relativistic phase. If, however, the somewhat larger estimate of total energy in the non-relativistic phase is indeed true, then two possible explanations may be advanced for this: either the beaming angle in relativistic phase is underestimated, giving a smaller value for the beaming corrected energy; or $E_{\rm ST}$ is over-estimated because of non-isotropy in the emission coming from the blast wave in the non-relativistic phase. In the latter case it could be that the blast wave is not completely spherical

yet, but still the evolution is well described by the Sedov-Taylor solution, or that the blast wave is spherical, but the emission is not coming from the blast wave isotropically; in both cases the value of $E_{\rm ST}$ that we derived would be an over-estimation of the true value.

The energies that we and Frail et al. (2005b) derive indicate that our estimate of the relativistic beaming and the assumption that the blast wave becomes spherical at $t \simeq t_{\rm NR}$ are valid. The latter is important for testing the models that describe the lateral spreading of the collimated outflow after the jet-break time, when the Lorentz factor drops below the inverse of the half-opening angle of the jet. Some (semi-analytical) models (e.g. Rhoads, 1999) assume a very rapid sideways expansion of the jet with a lateral expansion velocity of the order of the velocity of light, resulting in an exponential growth of the jet half-opening angle with radius. Hydrodynamical simulations, however, show a very modest degree of lateral expansion as long as the jet is relativistic (for an extensive review, see Granot, 2007). In the latter model the the outflow is still strongly collimated when the blast wave becomes non-relativistic, while the first model predicts that the blast wave is (almost) spherical at $t \simeq t_{\rm NR}$, which is favoured by our analysis, since there is no significant change in temporal slopes after $t_{\rm NR}$.

4.4.2 Counter Jet Emission

As stated before some of the features seen in the afterglow light curves are well explained by invoking the hypothesis that the GRBs and their afterglows are due to a collimated outflow rather than a spherical fireball. Naturally, the collimated outflow or jet is bi-directional and the relativistic jets are pointed in opposite directions. Apart from the narrow collimation the relativistic beaming points the radiation in the direction of motion of the jets. As a result the radiation received from the forward

jet is expected to dominate over the radiation from the jet in opposite direction. Eventually when the jets become non-relativistic and emission is no longer strongly beamed away from us, a rebrightening in the radio light due to contribution from the counter jet is predicted at about $5 \times t_{NR}$ (Granot and Loeb, 2003; Li and Song, 2004).

Adoptiing our values of $t_{NR} \sim 60 - 80$ days the rebrightning is expected at $\sim 300 - 400$ days after the burst. From Figure 4.1, however, it is clear that such a feature has not been observed up to 3 years after the burst (which was also noted, with observations up to 2 years after the burst, by Pihlström et al., 2007). The calculations by Li and Song (2004) are valid for those observing frequencies at which the light curve peaks when the blast wave is still ultra-relativistic and narrowly collimated. This means that it can only be applied to the light curves at 8.4 GHz and higher frequencies. Even at these frequencies we do not seem to have detected any such feature, although it is hard to make definite statements about this, since observations at these frequencies are available only up to 360 days. The light curves at 2.3 GHz and lower frequencies are not expected to show this kind of re-brightening, because they peak at or after $t_{\rm NR}$.

Concluding, we can not say, from the light curves presented here, whether we have seen emission from the counter jet or not. The fact that we do not see a late-time re-brightening at high radio frequencies could be due to the fact that the outflow is not very narrowly collimated. A flattening of the peak of the light curves at low radio frequencies, caused by the emission coming from the counter jet, could be present, but the scatter in the data prevents us from stating any firm conclusions on this.

4.4.3 Equal Time of Arrival Surfaces

Consider an explosion which is isotropic in the frame of reference attached to the centre of the explosion. Consider an "outside" observer who is at rest with respect to the centre of explosion. It is obvious that the photons arriving simultaneously at the observer were not emitted simultaneously from the expanding surface. These photons were emitted at different times hence from different radii of the emitting surface called Equal Time of Arrival (ETA) surfaces. The photon arrival time in the observer frame is related to the photon emission time in the source frame and it can be shown that

$$dt_{\oplus} = dt^{src} - dr\frac{\mu}{c} \tag{4.11}$$

where $dt_{\oplus}$ and dt^{src} are the times in the observer's and source's frames of reference, respectively. $\mu = cos(\theta)$ and $dr\mu/c$ is the projected distance travelled by the expanding surface in time $dt_{\oplus}$ as seen by the observer. At any given time $t_{\oplus}$, it represents an ellipsoid (Rees, 1966) for a shell moving with a constant velocity $\beta\, c$,

$$R = \frac{\beta c t_{\oplus}}{1 - \beta\mu} \tag{4.12}$$

For an ultra-relativistically expanding surface this ellipsoid get significantly stretched in a forward direction. For a particularly interesting case of fireball shock wave with $\Gamma \propto R^{-3/2}$, where Γ is the Lorentz factor of the expanding surface it has been shown by Granot et al. (1999) that

$$R = \frac{c\ t_{\oplus}}{1 - \mu + 1/(8\Gamma^2)} \tag{4.13}$$

This shape resembles an elongated egg and Granot et al. (1999) refers to it as "the Egg". For a non-relativistically expanding surface with a large radius the Equal Arrival Time in the observer's frame of reference would not look as strongly elongated

as “the Egg" but mere light travel time across the two opposite ends would be so large that it would not be spherical.

Consider a the shock wave generated during the GRB which was initially moving at ultra-relativistic speeds and having slowed down to the non-relativistic speed at late times. The size of the fireball bounded by such a shock wave is $\sim 10^{18}$ cm and the light travel time across the fireball $\sim$ year. Thus a photon emitted from the front end of such a fireball would be simultaneous in the observer's frame with a photon emitted about a year before from the opposite side of the fireball. At any given time $T_{\oplus}$, the surface of a fireball moving with velocity $\beta(r)\, c \propto r^{-a}$ is obtained by integrating Equation 4.11 and it is given by

$$T_{\oplus} - t_{NR} = \frac{R_{NR}}{\beta_{NR}\, c\, (1+a)} \left[\left(\frac{R}{R_{NR}} \right)^{1+a} - 1 \right] - \frac{\mu}{c} \left[R - R_{NR} \right] \tag{4.14}$$

where t_{NR} is the time of NR transition, R_{NR} and β_{NR} are, respectively, the corresponding radius and velocity (in units of c) of the shock front.

At any given time this surface, as discussed before, is not a sphere. The radiation coming from such a fireball has to be integrated over the volume bounded by this surface which will make the spectra and light curve in the NR regime smooth.

It is widely believed that the GRBs, instead of being isotropic, could be collimated. As the shock wave decelerates and significant lateral spreading of matter takes place, it is believed to become spherical though it is not clear if it becomes spherical by the time of NR transition or much later and this could have important bearing on the shapes of spectra and light curves and also on the estimates of energy outputs from GRBs.

We have calculated emission from such a fireball by taking into account ETA surfaces. Also, we have introduced an asymmetry parameter to check the effects of asymmetry on the afterglow light curves. To achieve a gradual and tunable

dependence of flux on θ we use a heuristic functional form of asymmetry parameter

$$\zeta = \frac{[\epsilon + cos^2(\theta)]}{2\ [\epsilon + 1/3]} \tag{4.15}$$

The factor in denominator is due to normalisation of the numerator : $\int_0^\pi \zeta\ sin\theta\ d\theta = 1$. The resultant light curves are plotted in Figure 4.2. A qualitative comparison of the plots with the observed light curve can be summarised as follows :

- The observed light curves are smooth. Hence, the light curves calculated by taking into account radiation only along the line of sight is not a correct representation of the reality. The emission estimates from ETA surfaces is closer to the real afterglow behaviour.

- The asymmetry of the fireball i.e. its deviation from sphericity manifests strongly at the peak of its brightness.

- The peak of the light curve, when integrated over the ETA surface, gets stretched over time axis by about a factor of two, compared to the light curve due to a point source (see Figure 4.2 and also Figure 4.1). To model observed light curves we have used power law light curve smoothened over time : $F = F_{peak}[(t/t_b)^{-\alpha_1\ s} + (t/t_b)^{-\alpha_2\ s}]^{-1/s}$ which emulates this effect. To distinguish between the degree of asymmetry one requires superior quality data without a scatter as present in the available data.

- The light curve shape is not very sensitive to the functional form used in present calculations. But the asymmetry of the fireball could be estimated, perhaps by using different functional forms of asymmetry, and with a finer temporal sampling of the data.

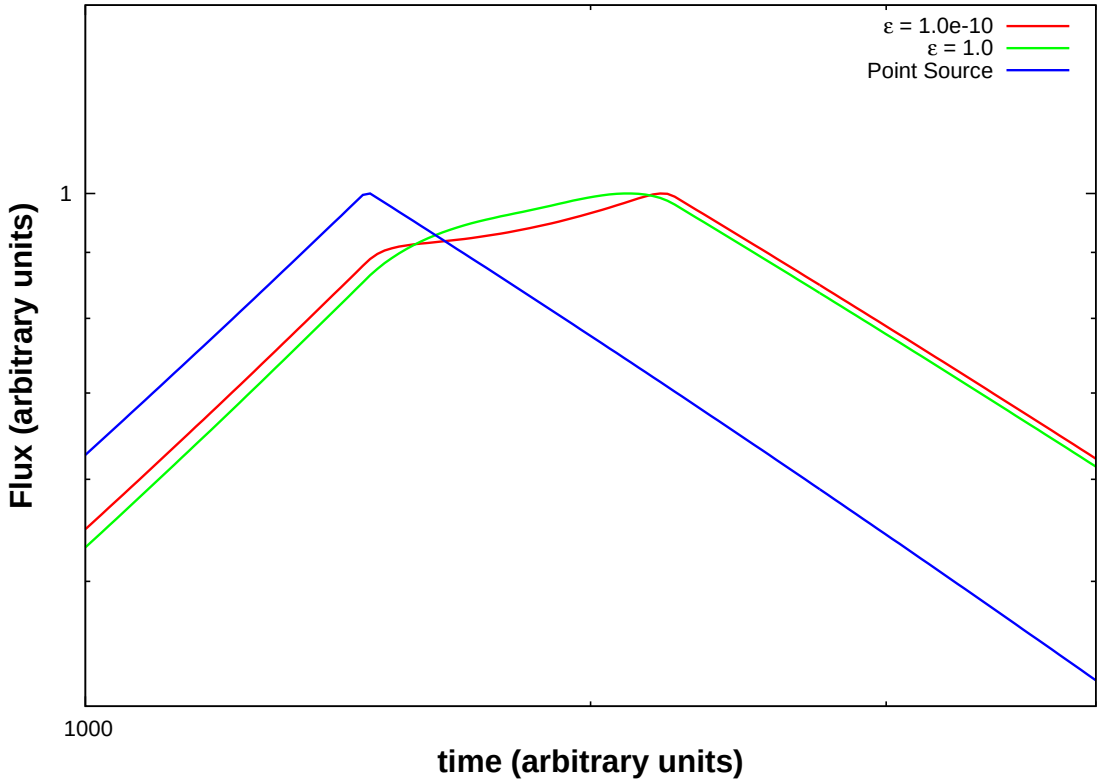

Figure 4.2: **Low frequency afterglow light curve due to an asymmetric fireball expanding with NR speeds :** The expected light curves due to different degrees of fireball asymmetry and integrated over the ETA surface. Consider the line corresponding to the light curve from a point source, – it is as though the entire emission was emerging from a single point source advancing towards the observer. In this case the light curve has a sharp peak and peaks relatively early as compared to the light curve due to emission from ETA surface of the fireball. Similarly, a light curve due to a receding point source would peak later – at the epoch corresponding to the secondary peak of the asymmetric fireball. The observed light curves have broadened smooth peaks (see Figure 4.1) which represents a case of emission from the entire surface instead of from a point source and peaks at intermediate times. All the light curves are normalised to their peak flux values.

4.4.4 Source Size Evolution

Apart from the light curve evolution, evolution of the fireball image size can provide important information about the fireball. The full set of VLBI measurements of GRB 030329 afterglow up to 806 days after the burst has been presented in Pihlström et al. (2007). Using the evolution of the fireball image size, Granot et al. (2005) concludes that the a homogeneous circum-burst medium gives a better fit than the wind. However, given the uncertainties in the available measurements wind circum-burst medium can not be ruled out in the case of GRB 030329. Furthermore, they try to constrain the epoch of NR transition using two different models : 1) considering rapid lateral spreading leading to early jet break in which they conclude $t_j \sim 1$ month and $t_{NR} \sim 1$ year and 2) considering no significant lateral spreading until the blast wave becomes non-relativistic. Since the jet break time, $t_j \sim 13$ days, is estimated to a better accuracy using multiband light curves, their estimates of $t_j and t_{NR}$ from model 1 are rather uncertain. The models in which there is no lateral expansion until the blast wave becomes non-relativistic, their model 2, the non-relativistic transition actually happens at 60-80 days after the burst; the blast wave then becomes spherical on a time scale of 1-3 years. So from the fits of model 2 it is clear that $t_{\rm NR} \sim 60 - 80$ days indeed.

4.5 Summary

GRB 030329 presented an unprecedented information about GRB fireballs and their evolution. As pointed out before, GRB 030329 displayed the brightest afterglow ever. Radio afterglow of GRB 030329 is the longest observed afterglow ever. It was also the afterglow observed at the lowest frequency, 610 MHz using GMRT.

- In this Chapter, we have presented a detailed study of the late-time radio

afterglow of GRB 030329. We have obtained measurements with the GMRT, at 325 MHz, 610 MHz and 1280 MHz with a wide temporal coverage up to 1400 days after the burst. Together with all the already published radio observations of this afterglow, from WSRT, GMRT and other large radio telescopes, we have studied the physics of the blast wave in the non-relativistic phase.

- The well-sampled late-time light curves made it possible to determine and compare various physical parameters of the fireball during relativistic and non-relativistic phase. We estimated the index of the electron energy distribution $p = 2.1$, and that the circumburst medium is homogeneous. We could also estimate the epoch of non-relativistic transition to be ~ 60 days after the burst. Using evolution of the afterglow during the non-relativistic phase the energy of the blast wave was estimated to be 8.2×10^{50} erg and the density of the circumburst medium ~ 1.3 cm^{-3}. These are comparable to findings by several studies on earlier time observations.

- We have shown that the blast wave, as seen by an outside observer, would not be spherical during the non-relativistic evolution and that the correct model should take into the ETA surfaces to model the evolution of GRB afterglows in non-relativistic phase. It is possible that the difference in the estimates of blast-wave energy could be due to a slight deviation of the fireball from sphericity. We compared, albeit qualitatively, the observed afterglow light curves with those expected from ETA surfaces of non-relativistic fireball.

- In contrast with some predictions, a radio re-brightening due to the counter jet becoming non-relativistic, is not observed. The existence of a counter jet can not be ruled out, since it is possible that the peaks of the light curves at low radio frequencies are flattened due to this counter jet. We have also

shown that the high-resolution VLBI measurements of the afterglow image size are in agreement with our light curve studies. In particular, the value of $t_{\rm NR}$ derived from modeling the image size evolution does not differ from our findings significantly.

Bibliography

Berger E., Kulkarni S.R., Pooley G. et al. Nature, 426, 154 (2003).

Frail D.A., Soderberg A.M., Kulkarni S.R. et al. ApJ, 619, 994 (2005a).

Frail D.A., Soderberg A.M., Kulkarni S.R. et al. ApJ, 619, 994 (2005b).

Frail D.A., Waxman E. and Kulkarni S.R. ApJ, 537, 191 (2000).

Galama T.J., Vreeswijk P.M., van Paradijs J. et al. A&AS, 138, 465 (1999).

Gorosabel J., Castro-Tirado A.J., Ramirez-Ruiz E. et al. ApJ Lett, 641, L13 (2006).

Granot J. Revista Mexicana de Astronomia y Astrofisica, vol. 27, volume 27 of Revista Mexicana de Astronomia y Astrofisica, vol. 27, 140–165 (2007).

Granot J. and Loeb A. ApJ Lett, 593, L81 (2003).

Granot J., Piran T. and Sari R. ApJ, 513, 679 (1999).

Granot J., Ramirez-Ruiz E. and Loeb A. ApJ, 618, 413 (2005).

Hjorth J., Sollerman J., Møller P. et al. Nature, 423, 847 (2003).

Kuno N., Sato N., Nakanishi H. et al. PASJ, 56, L1 (2004).

Li Z. and Song L.M. ApJ Lett, 614, L17 (2004).

Lipkin Y.M., Ofek E.O., Gal-Yam A. et al. ApJ, 606, 381 (2004).

Matheson T., Garnavich P.M., Stanek K.Z. et al. ApJ, 599, 394 (2003).

Pihlström Y.M., Taylor G.B., Granot J. and Doeleman S. ArXiv e-prints, 704 (2007).

Rao A.P., Ishwara-Chandra C.H. and Bhattacharya D. GRB Coordinates Network, 2073, 1 (2003).

Rees M.J. Nature, 211, 468 (1966).

Resmi L., Ishwara-Chandra C.H., Castro-Tirado A.J. et al. A&A, 440, 477 (2005).

Rhoads J.E. ApJ, 525, 737 (1999).

Sheth K., Frail D.A., White S. et al. ApJ Lett, 595, L33 (2003).

Stanek K.Z., Matheson T., Garnavich P.M. et al. ApJ Lett, 591, L17 (2003).

Tiengo A., Mereghetti S., Ghisellini G. et al. A&A, 409, 983 (2003).

van der Horst A.J., Kamble A., Resmi L. et al. ArXiv e-prints, 706 (2007).

van der Horst A.J., Rol E., Wijers R.A.M.J. et al. ApJ, 634, 1166 (2005).

Vanderspek R., Sakamoto T., Barraud C. et al. ApJ, 617, 1251 (2004).